A Spatiotemporal Comparison and Assessment of Multisource Satellite Derived Sea Ice Thickness in the Arctic Thinner Ice Region

Yu Zhang ⓘ, *Member, IEEE*, Guohao Li ⓘ, Huan Li ⓘ, Changsheng Chen ⓘ, Weizeng Shao ⓘ, *Member, IEEE*, Yi Zhou ⓘ, and Deshuai Wang ⓘ

Abstract—The accuracy and reliability of the latest version of multisource satellite derived Arctic sea ice thickness (SIT) in thinner ice regions are currently uncertain. This study integrated a comprehensive comparison and assessment of Arctic SIT derived from CryoSat-2, Soil Moisture and Ocean Salinity (SMOS), fusions of CryoSat-2 and SMOS (CS2SMOS), and Ice, Cloud, and Land Elevation Satellite-2 (ICESat-2) during 2011–2022. The focus was on the region with mean SIT less than 1 m. The five datasets from the Operation IceBridge L4 and Quick Look, IceBird campaign, CryoSat Validation Experiment, and the Canadian Arctic Archipelago stations were utilized as the reference data in the assessment. The four satellite products could capture similar major spatiotemporal variations in SIT. During 2011–2022, CryoSat-2 generally derived the largest multiyear mean SIT, followed by CS2SMOS, and SMOS exhibited the smallest mean. During 2018–2022, ICESat-2 recorded the largest mean SIT and the rankings of the other three satellite products remained consistent. The comparison and assessment results indicated that all four satellite products generally exhibited some underestimations of SIT. During 2011–2022, the comprehensive results highlighted CryoSat-2 as the best overall performance product, exhibiting optimal agreement with all five reference datasets. During 2018–2022, CryoSat-2 consistently demonstrated the best overall performance. CS2SMOS exhibited

Yu Zhang is with the College of Oceanography and Ecological Science, Shanghai Ocean University, Shanghai 201306, China, and also with the Southern Marine Science and Engineering Guangdong Laboratory (Zhuhai), Zhuhai 519082, China (e-mail: yuzhang@shou.edu.cn).

Guohao Li, Huan Li, and Weizeng Shao are with the College of Oceanography and Ecological Science, Shanghai Ocean University, Shanghai 201306, China (e-mail: m220200614@st.shou.edu.cn; m230200643@st.shou.edu.cn; wzshao@shou.edu.cn).

Changsheng Chen is with the School for Marine Science and Technology, University of Massachusetts-Dartmouth, New Bedford, MA 02744 USA (e-mail: c1chen@umassd.edu).

Yi Zhou is with the College of Oceanography and Ecological Science, Shanghai Ocean University, Shanghai 201306, China, and also with the School of Oceanography, Shanghai Jiao Tong University, Shanghai 200030, China (e-mail: yizhou.os@sjtu.edu.cn).

Deshuai Wang is with the School for Marine Science and Technology, University of Massachusetts Dartmouth, New Bedford, MA 02744 USA, and also with the Horn Point Laboratory, University of Maryland Center for Environment Science, Cambridge, MD 21613 USA (e-mail: wangd@umces.edu).

Digital Object Identifier 10.1109/JSTARS.2024.3390618

a performance similar to CryoSat-2 in the two selected periods. This study contributes to further understandings of reliabilities and potential disparities among the latest versions of multisource satellite products in the thinner ice region.

Index Terms—Arctic, assessment, comparison, satellite, sea ice thickness (SIT), thin ice.

I. INTRODUCTION

ARCTIC sea ice, an important indicator of global climate change, plays a critical role in the albedo effect, oceanic and atmospheric circulation, regulation of heat exchange, biological activity, and freshwater balance, exerting a profound influence on the Earth's climate system [1], [2], [3], [4], [5], [6]. In the past decades, the Arctic sea ice has declined significantly with the retreat of sea ice cover, reduction of sea ice thickness (SIT), and the acceleration of sea ice drift through the changes in the annual sea ice freeze–thaw cycle [7], [8], [9], [10], which has resulted in increased opportunities for maritime activities [11], [12].

Compared with the data on Arctic sea ice concentration and sea ice drift, the available SIT data are limited in spatiotemporal scales [13], [14], [15]. Presently, various methods are employed to measure SIT, encompassing drill holes, upward looking sonars, sea ice mass balance buoys, airborne observations equipped with radar and laser altimeters, as well as electromagnetic methods [16], [17], [18], [19], [20]. However, these measurement methods face challenges in achieving relatively complete spatiotemporal coverage of SIT. The advancements in satellite products featuring high spatial resolution, extensive measurement range, and long time series are extensively applied in studies related to sea ice [21], [22], [23], [24]. Over the last two decades, several satellite-derived SIT products have been developed. The Ice, Cloud, and Land Elevation Satellite (ICESat), equipped with a precision laser altimeter system, covered the observational period from 2003 to 2008 [25]. The CryoSat-2 product, featuring a synthetic aperture radar/Interferometric Radar Altimeter, was initiated in 2010 [26]. The SIT data of the Soil Moisture and Ocean Salinity (SMOS) satellite was carried out in 2010 [27]. The CS2SMOS product, a fusion of CryoSat-2 and SMOS data, was developed by the Alfred Wegener Institute (AWI) and the University of Hamburg [28]. The ICESat-2 was launched by the National Aeronautics and Space Administration (NASA) and the measurement was commenced in 2018 [29].

However, these products exhibit noticeable measurement discrepancies in the derived SIT owing to differences in measurement instruments and retrieval methods, in particular over the region with thinner ice. Considering a 1-m SIT threshold was employed as the criterion for identifying thin ice when merging CryoSat-2 and SMOS data into CS2SMOS, and the SMOS relative uncertainties are lowest for thin ice (< 1 m) [28], the region where the mean SIT derived from SMOS is less than 1 m during January–April and October–December from 2011 to 2022 is defined as thinner ice region in this study. The Arctic thinner ice region, characterized by significant sea ice melting and freezing processes, exhibits sensitive responses to climate change. Due to the inverse relationship between SIT and its insulative properties, the heat loss in the thinner ice region during winter is significantly greater, ranging from one to two orders of magnitude, compared to thicker ice areas [30].

A few studies have been undertaken to compare disparities among various satellite-based SIT products including CryoSat-2, SMOS, CS2SMOS, and ICESat-2, but most studies have only involved the comparison of a limited number of satellite product types, typically no more than three types [31], [32], [33], [34], [35], [36], [37], [38]. The types of measurement data used as the assessment reference are also restricted, leading to a scarcity of comprehensive comparison and assessment of multisource satellite derived products. In addition, a noteworthy development is the recent version upgrade of SIT retrieval for CS2SMOS, CryoSat-2, and ICESat-2 in October, November, and December 2023, respectively. Majority of the current studies were focused on Arctic-wide comparisons and previously released data versions, with limited emphasis on the thinner ice region and the latest product version. It remains unclear about the accuracy and reliability of the latest data version, the extent of disparities among satellite products in the thinner ice region, and the degree of alignment with other observational data.

Therefore, this study, for the first time, integrated a spatiotemporal comparison and assessment of the latest versions of diverse satellite products from CryoSat-2, SMOS, CS2SMOS, and ICESat-2 over the period 2011–2022, with a specific focus on the thinner ice region. Four types of datasets from airborne and in situ measurements were used comprehensively in the assessment as the reference data. The comparison and assessment of multisource satellite derived SIT facilitates the validation and calibration of satellite products, aiding in the refinement of algorithms and methodologies used in SIT retrieval in the thinner ice region. This, in turn, provides valuable insights into the vulnerability in the Arctic thinner ice region and the response of the region to climate change.

II. DATA AND METHOD

A. Satellite Data

1) CryoSat-2: In this study, the latest version 2.6 of monthly CryoSat-2 SIT data released in November 2023 from AWI was selected [39]. CryoSat-2 covers the sea ice growth season from October to April. The spatial resolution of CryoSat-2 is 25 km and the period used is from January 2011 to December 2022.
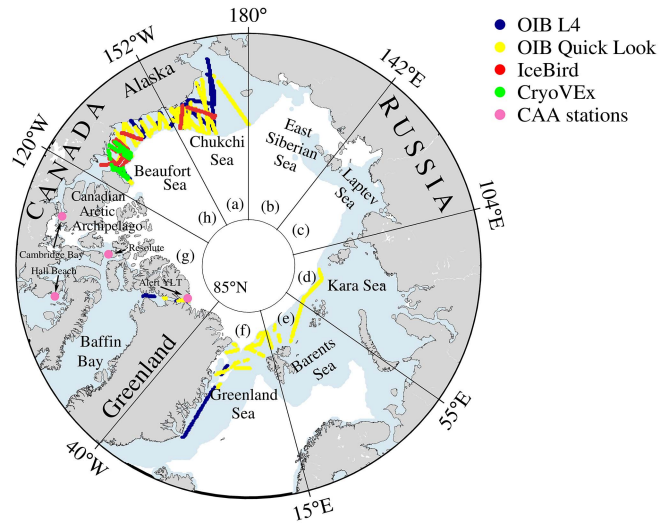

Fig. 1. Distribution of the assessment data and the division of Arctic thinner ice region. The subregions encompass the following. (a) Chukchi Sea. (b) East Siberian Sea. (c) Laptev Sea. (d) Kara Sea. (e) Barents Sea. (f) Greenland Sea. (g) Canadian Arctic Archipelago. (h) Beaufort Sea. Blue shading indicates the defined thinner ice region in this study.

2) SMOS: The latest version 3.3 of daily SMOS SIT data released in November 2021 from AWI was utilized [40]. SMOS has a spatial resolution of 12.5 km and also covers the sea ice growth season from October to April. The study period is the same as CryoSat-2.

3) CS2SMOS: Since the weekly CS2SMOS SIT data was developed by AWI based on the fusion of CryoSat-2 and SMOS, it can maintain the same study period with CryoSat-2 and SMOS [28]. The spatial resolution is 25 km and the latest version 206 released in October 2023 was used.

4) ICESat-2: The latest version 3 of monthly ICESat-2 SIT data released in December 2023 from the National Snow and Ice Data Center (NSIDC) was used in the study [41]. ICESat-2 also encompasses the sea ice growth season, spanning from October to April. The study period is from November 2018 to December 2022. The spatial resolution is 25 km.

B. Reference Data in the Assessment

1) Operation IceBridge (OIB): The OIB SIT was retrieved from the IceBridge Airborne Topographic Mapper, Snow Radar, Digital Mapping System, Continuous Airborne Mapping By Optical Translator, and KT19 pyrometer. Two versions including OIB L4 [42] and OIB Quick Look [43] were used in the study. The OIB L4 dataset covers the period from 2011 to 2013 and has been validated to demonstrate consistency with independent datasets [19]. Although the OIB Quick Look dataset has an additional uncertainty, it contains a longer observational period than OIB L4. The OIB Quick Look with the period over 2014–2019 was included. The tracks of OIB L4 and OIB Quick Look are shown in Fig. 1.

2) IceBird Campaign (IceBird): AWI IceBird campaign series were measured in 2017 [44] and 2019 [45]. For each flight, the geolocated total thickness data (sum of SIT and snow depth)

and snow depth from an airborne electromagnetic induction sensor are provided with a point spacing of approximately 5–6 m. According to the AWI validation report, the uncertainty of IceBird is approximately 0.1 m for level ice [46]. The snow depth from IceBird is subtracted from the total to acquire the SIT data. The tracks of IceBird are shown in Fig. 1.

3) CryoSat Validation Experiment (CryoVEx): The Cry- oVEx was performed with airborne electromagnetic and laser measurements to compute total thickness in 2014 [47]. The ice thickness distributions of CryoVEx are in relatively good agreement with drill hole data both in the Beaufort Sea and north of Greenland. CryoVEx data agrees well with OIB data over the Greenland ice camp. In order to estimate the SIT data, the snow depth derived from the Chinese Feng Yun-3 satellite with the MicroWave Radiometer Imager (FY3/MWRI) [48] was used to be subtracted from the total thickness. The snow depth data had been validated and exhibited smaller biases when compared to the OIB data. The tracks of CryoVEx are shown in Fig. 1.

4) Canadian Arctic Archipelago Stations (CAA Stations): The in situ SIT observation from the CAA stations during 2011–2022 can be obtained from the Canadian Ice Service. Four sites of Cambridge Bay, Resolute, Hall Beach, and Alert YLT were selected (Fig. 1). The measurements are primarily collected using drill holes at nearly identical locations each year on a weekly basis. This process begins after freeze-up when the ice is safe to walk on and continues until break-up or when the ice becomes unsafe. This limitation leads to incomplete measurements at certain sites.

C. Comparison of Satellite Products

To maintain consistency in comparing different satellite products, all the SIT datasets were averaged into monthly mean data and interpolated to generated grids with a resolution of 12.5×12.5-km north of 65°N. This interpolation has been performed using the inverse distance weighting (IDW) method, addressing disparities in spatiotemporal resolution among the various satellite products.

Given that the sensitivity of SMOS diminishes when the ice thickness exceeds 1 m, the thinner ice region is determined by the mean SIT of SMOS over the period 2011–2022 which is less than 1 m. Due to the different available periods of these satel- lite products, the comparison time periods are categorized into two sets: 1) the comparison involving CryoSat-2, SMOS, and CS2SMOS spanning from 2011 to 2022, and 2) the comparison involving CryoSat-2, SMOS, CS2SMOS, and ICESat-2 for the period from 2018 to 2022.

In order to compare the regional disparities of these satellite products, the thinner ice region is divided into eight subregions: 1) Chukchi Sea, 2) East Siberian Sea, 3) Laptev Sea, 4) Kara Sea, 5) Barents Sea, 6) Greenland Sea, 7) the CAA and Baffin Bay, and 8) Beaufort Sea (Fig. 1). The metrics of Bias, root mean squared error (RMSE), and correlation coefficient (CC) were used in the comparisons of various satellite products to examine their agreements and similarities.
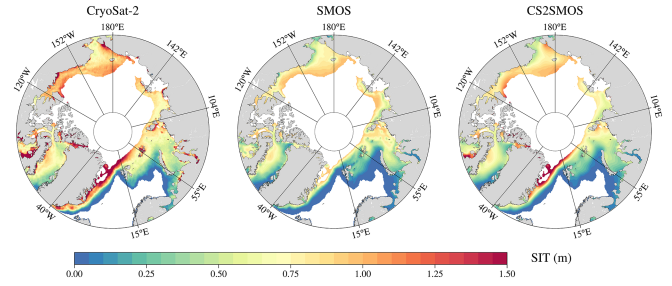

Fig. 2. Spatial distribution of multiyear mean SIT for CryoSat-2, SMOS, and CS2SMOS over the period 2011–2022.

D. Assessment of Satellite Products

The assessment time periods of satellite products are also cat- egorized into the same two sets, 2011–2022 and 2018–2022. In the assessment of multisource satellite SIT using OIB, IceBird, and CryoVEx data, we followed the method used in [49]. We utilized the same generated grids as those employed for satellite products and calculated the gridded mean of OIB, IceBird, and CryoVEx by averaging the reference data within a 12.5-km radius of each generated grid. Besides, we additionally evaluated the SIT from multisource satellites along some long trajectories of OIB by using the approach in [50]. Data grids are generated at 12.5-km intervals along the trajectories of OIB. The mean SIT of OIB for each data grid is calculated by averaging the OIB data within a 12.5-km range along the trajectory. Satellite data are interpolated onto these data grids using the IDW method. In the assessment of multisource satellite SIT with the CAA stations data, the satellite data are interpolated to the location of the stations by the IDW method.

The assessment employed metrics including Bias, RMSE, CC, and distance between indices of simulation and observation (DISO). In this study, bias is defined as the mean difference between satellite data and reference data. DISO provides a versatile approach for determining statistical metrics and their numbers [51]. A lower DISO value represents a higher ranking. In this study, we established a composite metric that integrates three statistical metrics of Bias, RMSE, and CC to assess the performance of satellite products. The equation of DISO is defined as

$$\text{DISO}_i = \sqrt{\text{NBias}_i^2 + \text{NRMSE}_i^2 + (\text{NCC}_i - 1)^2} \quad (1)$$

where $i = 0, 1, \ldots, m$, 0 indicates the observational data, and m is the total number of satellite products. NBias, NRMSE, and NCC indicate the normalized metrics of Bias, RMSE, and CC, respectively. Bias, RMSE, and CC are normalized to be between 0 and 1 and the normalization equation is expressed as

$$\text{NM}_i = \frac{M_i - \min(M)}{\max(M) - \min(M)} \quad (2)$$

where M indicates the metric, such as Bias, RMSE, and CC. When $i = 0$, the metrics of Bias, RMSE, and CC between the observational data and itself are 0, 0, and 1, respectively. The overall performance of satellite products is assessed by
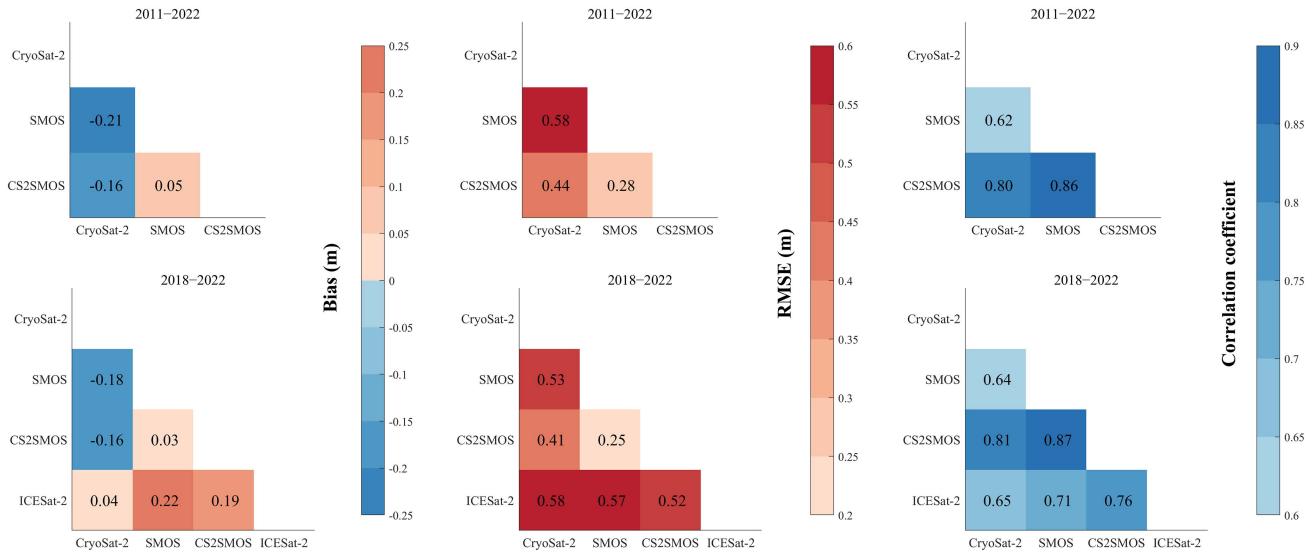
Fig. 3. Bias, RMSE, and CC of SIT between the satellite products, calculated using all spatial monthly samples over the period 2011–2022 and 2018–2022. Bias is defined as the difference between the satellite products of the Y-axis and X-axis.
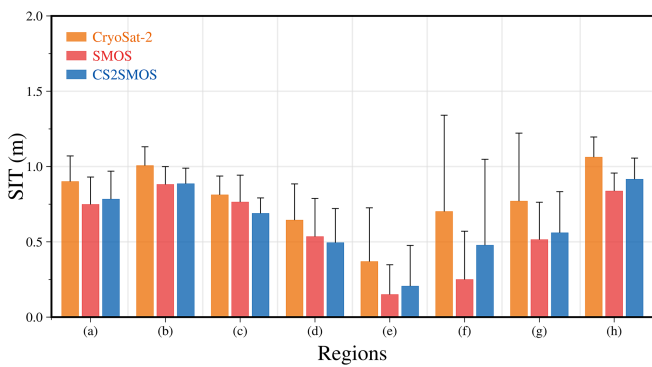

Fig. 4. Multiyear mean SIT in the subregions for CryoSat-2, SMOS, and CS2SMOS over the period 2011–2022. The black vertical bar indicates the positive range of standard deviation. The subregions comprise: (a) Chukchi Sea, (b) East Siberian Sea, (c) Laptev Sea, (d) Kara Sea, (e) Barents Sea, (f) Greenland Sea, (g) Canadian Arctic Archipelago, and (h) Beaufort Sea, identical to those illustrated in Fig. 1.

combining all of the reference data from different datasets and calculating DISO.

III. COMPARISONS OF MULTISOURCE SATELLITE DATA

A. CryoSat-2, SMOS, and CS2SMOS Over 2011–2022

The multiyear mean SIT for CryoSat-2, SMOS, and CS2SMOS over the period 2011–2022 showed reasonable agreement of major spatial distribution patterns (Fig. 2). CryoSat-2 indicated the largest mean SIT among three satellite products. CS2SMOS showed the second largest result, and the smallest SIT was for SMOS. The lowest bias, lowest RMSE, and highest CC between CS2SMOS and SMOS suggested that CS2SMOS had a closer agreement with SMOS than with CryoSat-2 in the thinner ice region (Fig. 3). In the subregions, CryoSat-2 and CS2SMOS showed the largest mean SIT in the
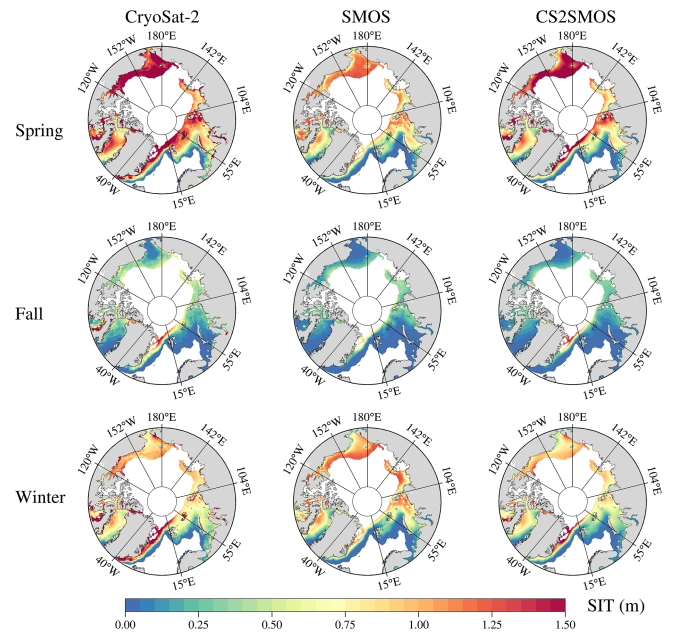

Fig. 5. Spatial distribution of seasonal mean SIT for CryoSat-2, SMOS, and CS2SMOS over the period 2011–2022.

Beaufort Sea, while SMOS displayed the largest values in the East Siberian Sea (Fig. 4). All the three satellite products indicated the Barents Sea as the subregion with the smallest mean SIT. In terms of the seasons, the ranking of three satellite products in relation to seasonal mean SIT remained consistent (Fig. 5). All three satellite products indicated that the region of Barents Sea with the minimum seasonal mean SIT was the same as the region highlighted by the multiyear mean SIT. Nevertheless, some distinct variations were observed in the regional characteristics of maximum seasonal mean SIT. In spring
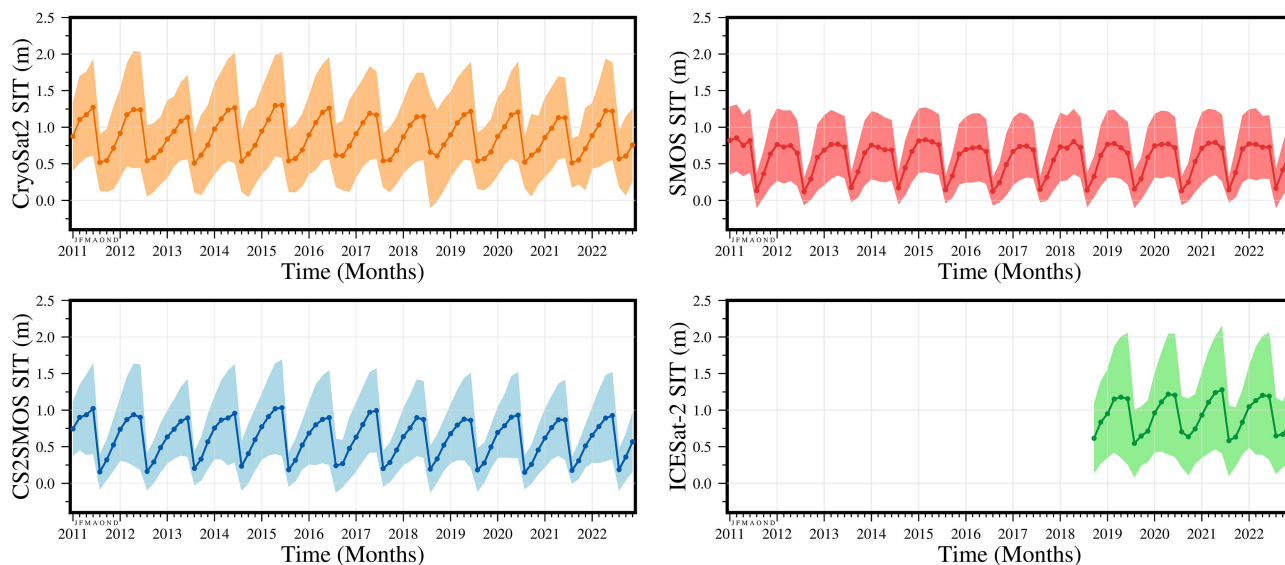
Fig. 6.   Monthly variations of spatial mean SIT for CryoSat-2, SMOS, CS2SMOS, and ICESat-2 over the period 2011–2022. The shading indicates the standard deviation of SIT for all the spatial samples.
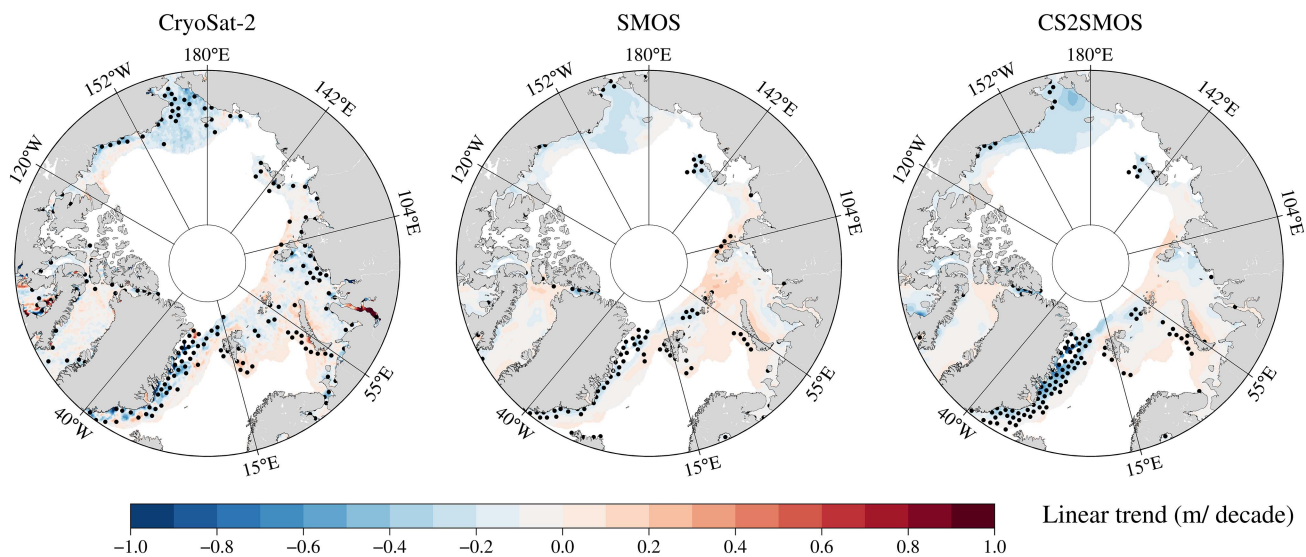

Fig. 7.   Linear trend of SIT for CryoSat-2, SMOS, CS2SMOS, and ICESat-2 over the period 2011–2022. The black dots indicate the regression slopes at the 95% confidence level.

(March–April), SMOS showed the Chukchi Sea as the region with the maximum mean SIT. In fall (October–November), the location of the maximum thickness region shifted to the East Siberian Sea for CryoSat-2, and the Laptev Sea for SMOS and CS2SMOS. In winter (December–February), the region of maximum mean SIT for each satellite product was consistent with the region of multiyear mean.

The monthly variations of spatial mean SIT over the period 2011–2022 were highly correlated with the range of CC from 0.82 to 0.97 ($p < 0.01$) among the three satellite products (Fig. 6). Similar to the multiyear spatial mean findings, the time series mean SIT also suggested that CryoSat-2 exhibited the largest

mean SIT, followed by CS2SMOS with the second-largest result, while SMOS recorded the smallest SIT. Both SMOS and CS2SMOS typically showed the minimum SIT in October, while CryoSat-2 occasionally identified November as the month with the smallest SIT. In contrast, CryoSat-2 and CS2SMOS usually exhibited the maximum SIT during March–April, but SMOS sometimes identified January or February as the month with the largest SIT. All three satellite products exhibited very slight decreasing trends, implying that the SIT in the thinner ice region did not experience a substantial decline. In terms of spatial distribution, the regions with significant changes in SIT were primarily concentrated in the Atlantic sector (Fig. 7). All three
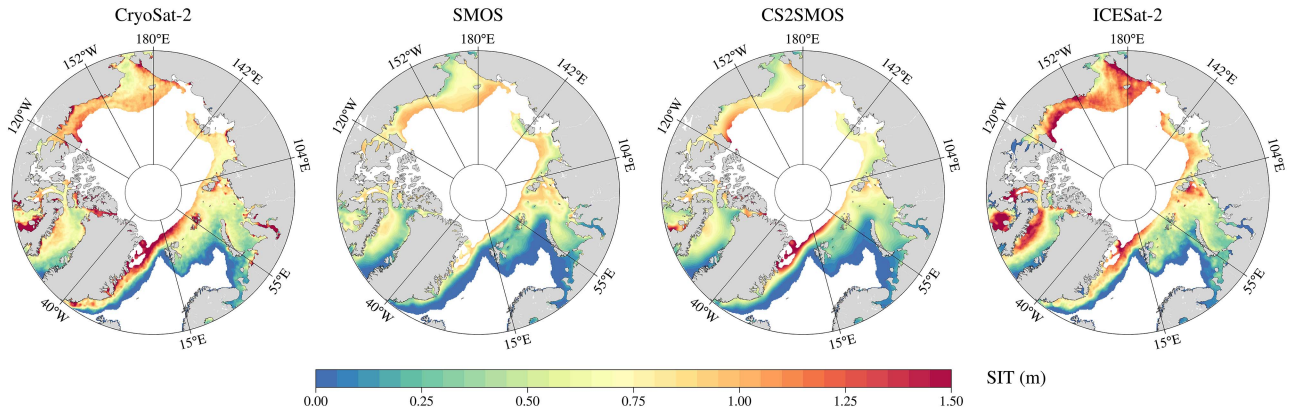
Fig. 8. Spatial distribution of multiyear mean SIT for CryoSat-2, SMOS, CS2SMOS, and ICESat-2 over the period 2018–2022.

satellite products indicated declines in SIT within the Greenland Sea region and CS2SMOS revealed the most extensive area with significantly reduced SIT. In the Pacific sector, all three satellite products indicated that reductions in SIT were primarily concentrated in the Chukchi Sea and CryoSat-2 showed the most extensive area.

B. CryoSat-2, SMOS, CS2SMOS, and ICESat-2 Over 2018–2022

Since 2018, with the inclusion of ICESat-2, the spatial distribution of multiyear mean SIT from four products indicated that ICESat-2 retrieved the maximum SIT, with CryoSat-2 following in the second place. CS2SMOS was in the third position, and SMOS exhibited the smallest thickness (Fig. 8). Based on the bias, RMSE, and CC results, in the thinner ice region, the similarity between CS2SMOS and SMOS was the highest, followed by the difference between CS2SMOS and CryoSat-2 as the second smallest, and the third closest agreement was observed between ICESat-2 and CS2SMOS (Fig. 3). In the subregions, all the four satellite products showed the largest mean SIT in the Beaufort Sea and the smallest mean SIT in the Barents Sea (Fig. 9).

In the different seasons, the ranking characteristics had a slight change. CryoSat-2 displayed a seasonal mean SIT in spring that was 0.02-m larger than ICESat-2, and SMOS showed a seasonal mean SIT in winter that was 0.04-m larger than CS2SMOS (Fig. 10). During all three seasons, the findings from all the four satellite products consistently identified the Barents Sea as the region with the smallest seasonal mean SIT, aligning with the region emphasized in the multiyear mean SIT results. Compared to the region where the multiyear mean SIT was maximum in the Beaufort Sea, all four satellite products consistently indicated that the region with the maximum winter mean SIT remained the Beaufort Sea. However, in spring, SMOS and ICESat-2 suggested that the region with maximum seasonal mean SIT shifted to the Chukchi Sea. In fall, CryoSat-2 and SMOS indicated a shift in the region with the maximum seasonal mean SIT to the East Siberian Sea and Laptev Sea, respectively.
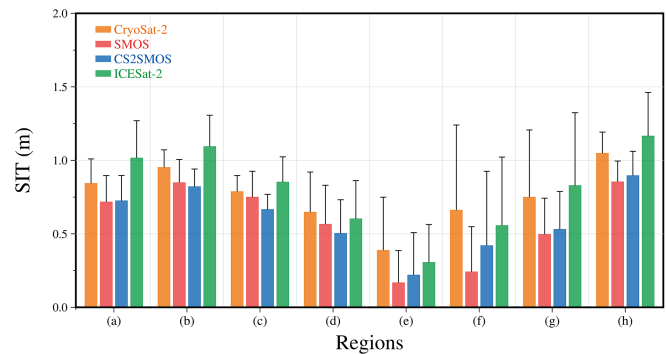

Fig. 9. Multiyear mean SIT in the subregions for CryoSat-2, SMOS, CS2SMOS, and ICESat-2 over the period 2018–2022. The black vertical bar indicates the positive range of standard deviation. The subregions comprise: (a) Chukchi Sea, (b) East Siberian Sea, (c) Laptev Sea, (d) Kara Sea, (e) Barents Sea, (f) Greenland Sea, (g) Canadian Arctic Archipelago, and (h) Beaufort Sea, identical to those illustrated in Fig. 1.

Over the period 2018–2022, the monthly variations of spatial mean SIT showed relatively high correlations with the range of CC from 0.82 to 0.98 ($p < 0.01$) among the four satellite products (Fig. 6). The time series mean SIT also indicated that ICESat-2 had the maximum SIT, with CryoSat-2 in the second place. CS2SMOS took the third position, and SMOS displayed the smallest thickness. CroySat-2, SMOS, and CS2SMOS exhibited very slight decreasing trends, while ICESat-2 showed very slight increasing trends. Further analyses of the spatial distribution of linear trend confirmed that the locations with significant changes in SIT were limited (Fig. 11). Notably, only CryoSat-2 and ICESat-2 primarily exhibited some areas with noticeable changes of SIT in the Atlantic sector.

IV. ASSESSMENTS OF MULTISOURCE SATELLITE DATA

The preceding comparative analysis of SIT enables us to quantify the extent of disparities among multisource satellite products. However, to evaluate the accuracy and reliability of the latest version of SIT, it is crucial to depend on the assessments with airborne and in situ measurement data.
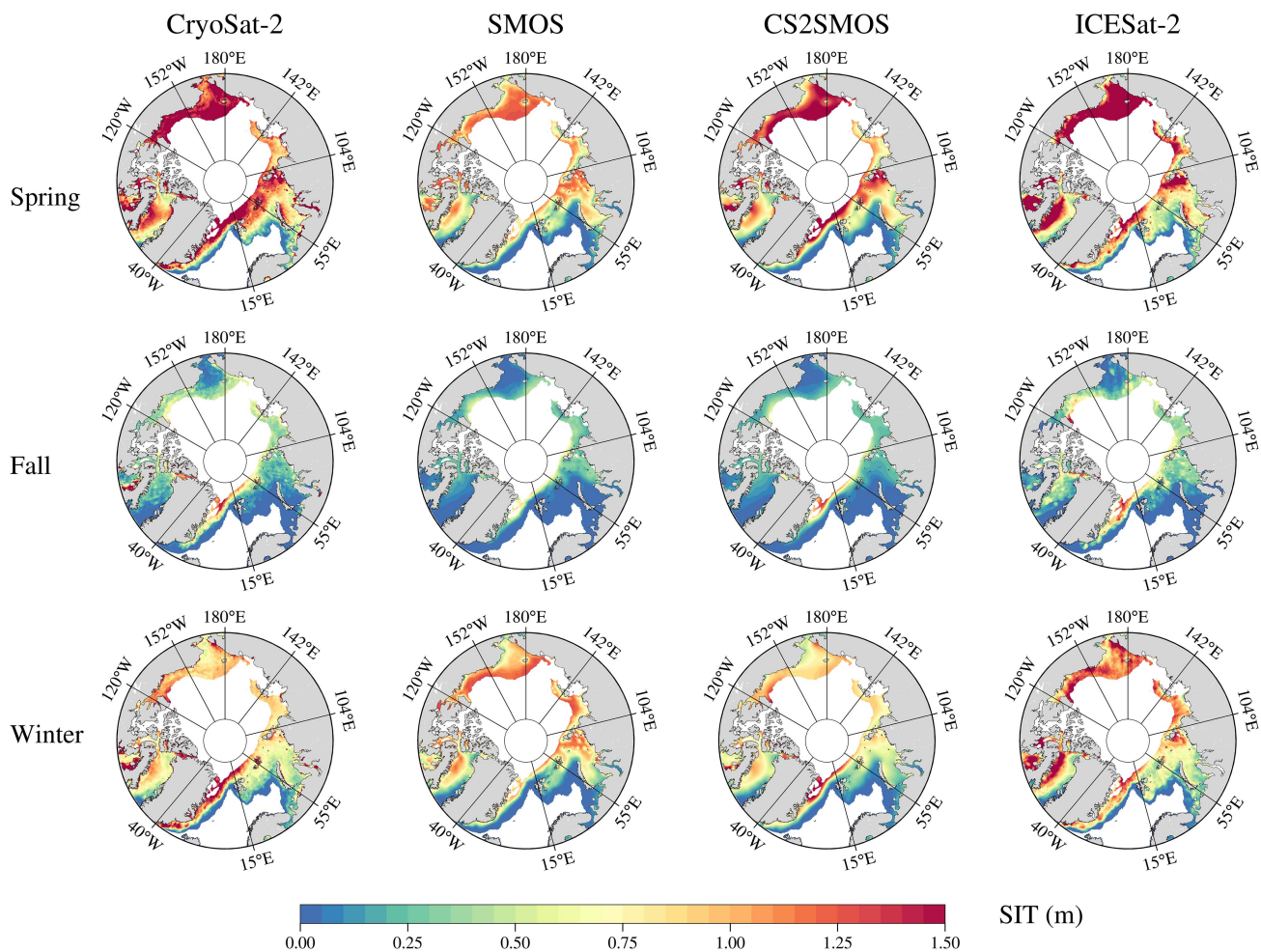
Fig. 10.   Spatial distribution of seasonal mean SIT for CryoSat-2, SMOS, CS2SMOS, and ICESat-2 over the period 2018–2022.
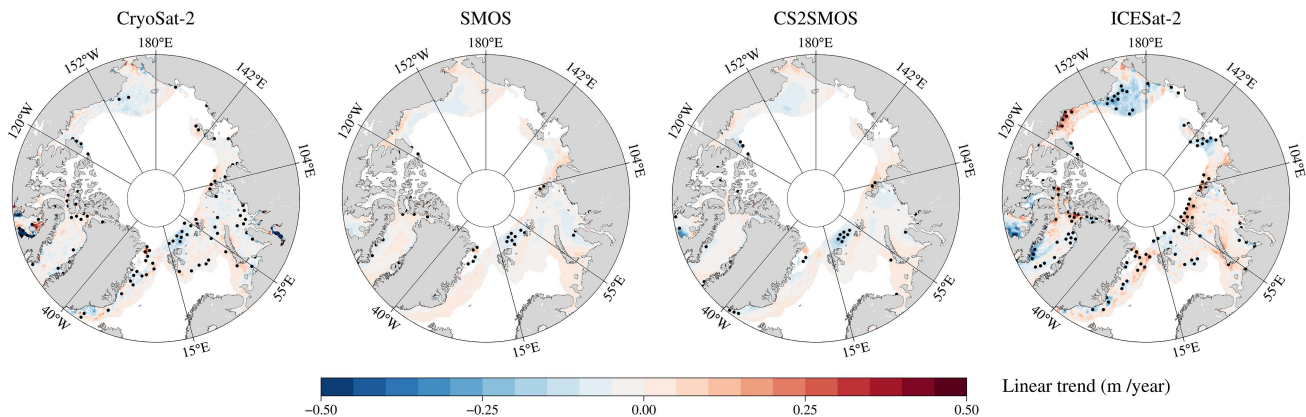

Fig. 11.   Linear trend of SIT for CryoSat-2, SMOS, CS2SMOS, and ICESat-2 over the period 2018–2022. The black dots indicate the regression slopes at the 95% confidence level.

TABLE I
DISO VALUES OF SATELLITE DERIVED SIT WITH VARIOUS REFERENCE DATASETS IN THE ASSESSMENT

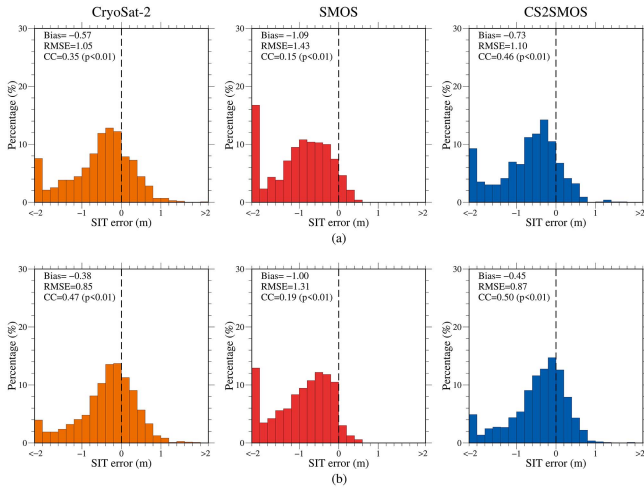|	2011−2022			2018−2022			
	CryoSat-2	SMOS	CS2SMOS	CryoSat-2	SMOS	CS2SMOS	ICESat-2
OIB L4	1.18	1.73	1.20	/	/	/	/
OIB Quick Look	0.99	1.73	1.02	1.04	1.65	1.12	1.14
IceBird	1.11	1.73	1.14	1.19	1.71	1.27	1.54
CryoVEx	1.25	1.55	1.40	/	/	/	/
CAA stations	1.23	1.61	1.42	1.00	1.24	1.15	1.71
Overall performance	1.09	1.73	1.14	0.78	1.73	0.83	1.18

Fig. 12. Assessment of satellite SIT derived from CryoSat-2, SMOS, and CS2SMOS with (a) OIB L4 data during 2011–2013 and (b) OIB Quick Look data during 2014–2019.

A. CryoSat-2, SMOS, and CS2SMOS Over 2011–2022

Over the period 2011–2013, the assessment of three satellite products with the OIB L4 reference data indicated that CryoSat-2, SMOS, and CS2SMOS generally underestimated SIT in some of the Alaska and Greenland coast regions. The CryoSat-2 exhibited the smallest mean negative error, with 75.6% of the samples showing negative errors, while the percentage of negative errors was 92.8% and 84.2% for SMOS and CS2SMOS, respectively [Fig. 12(a)]. Among the three products, CryoSat-2 showed the smallest DISO (Table I) with the lowest bias and RMSE [Fig. 12(a)], indicating the best match with OIB L4. The CS2SMOS showed a similar DISO to CryoSat-2 and had the highest CC with OIB L4. During 2014–2019, when compared with OIB Quick Look data, three satellite products also exhibited the underestimation of SIT and CryoSat-2 still demonstrated the smallest mean negative error [Fig. 12(b)]. The CryoSat-2 showed the smallest DISO of 0.99 and CS2SMOS showed the similar DISO of 1.02 (Table I). The SMOS always had the largest discrepancy with OIB data.

Further analyses were focused on the SIT variation along the flight trajectories of OIB (Fig. 13). The six longer trajectories from OIB L4 and Quick Look data in different regions and periods were selected as representative examples. The analysis results supported the major findings that all three satellite products mostly derived smaller mean SIT than the OIB data. Only

CS2SMOS exhibited a slight overestimation of mean SIT along the trajectory of April 2017. Furthermore, CS2SMOS generally demonstrated a relatively good performance among the three satellite products, with CryoSat-2 exhibiting better performance than CS2SMOS only along the trajectory in April 2012.

In the assessment with IceBird data in 2017 and 2019, the mean SIT in all three satellite products was underestimated [Fig. 14(a)]. CryoSat-2 showed the smallest DISO of 1.11 (Table I) with the lowest bias, lowest RMSE, and highest CC, thus suggesting the most favorable performance in comparison to the IceBird data. CS2SMOS demonstrated a DISO close to that of CryoSat-2, while SMOS displayed the least favorable match with the IceBird data.

When assessed with CryoVEx data in 2014, CryoSat-2 was the only satellite that showed a slight overestimation of mean SIT [Fig. 14(b)]. CryoSat-2 showed the smallest DISO. Despite SMOS displaying the highest CC, it displayed the highest bias and RMSE [Fig. 14(b)]. Consequently, this led to a larger DISO for SMOS compared to CS2SMOS (Table I).

In the assessment with the observational data from the CAA stations, due to differences in spatial coverage among the three satellite products, the time series of SIT data differs in the four stations. The assessment was focused on the common period of the derived datasets and the reference data. The SIT of all three satellite products was underestimated in the Resolute and Hall beach stations (Fig. 15). In addition, only SMOS overestimated SIT in the Cambridge Bay station and underestimated SIT in the Alert YLT station. According to the results of DISO, SMOS, and CS2SMOS displayed the optimal agreement of SIT with the Alert YLT and Cambridge Bay stations, respectively, and CryoSat-2 demonstrated the best match with the Resolute and Hall beach stations. Considering the common data from all stations, CryoSat-2 exhibited the best performance in SIT retrieval (Table I).

Based on the comprehensive assessment using the data of OIB L4, OIB Quick Look, IceBird, CryoVEx, and the CAA stations during 2011–2022, CryoSat-2 showed the best overall performance, and the CS2SMOS showed a close performance to CryoSat-2 (Table I).

B. CryoSat-2, SMOS, CS2SMOS, and ICESat-2 Over 2018–2022

Starting from 2018, ICESat-2 data were added into the assessment and the remaining available reference data only included OIB Quick Look, IceBird, and the CAA stations.
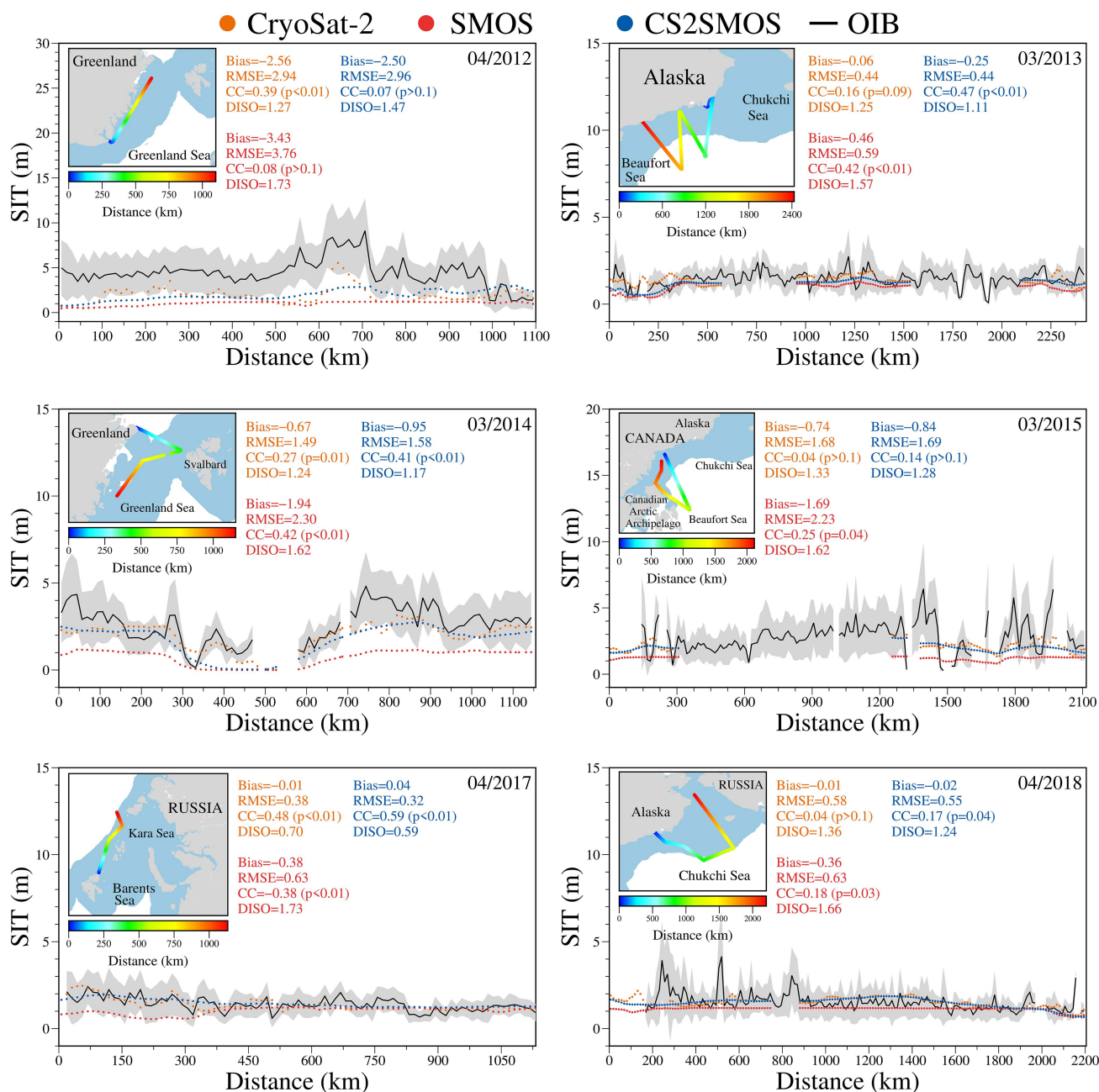
Fig. 13. Assessment of three satellite derived SIT with OIB L4 and Quick Look data along some OIB L4 and Quick Look trajectories. The OIB trajectory is shown in the small inserted figure, with the colors representing the distance from the starting position.

In 2019, compared with the OIB Quick Look data, the mean SIT in all the four satellite products were underestimated [Fig. 16(a)]. The CryoSat-2 showed the smallest DISO (Table I). CS2SMOS and ICESat-2 ranked second and third. SMOS exhibited relatively large discrepancies with the reference data, as both bias and RMSE exceeded 1 m.

In the assessment with IceBird data in 2019, all four satellite products also underestimated the mean SIT [Fig. 16(b)]. CryoSat-2 showed the best agreement with IceBird data, with CS2SMOS in the second place, and ICESat-2 in the third position (Table I).

For the CAA stations data, due to limited data during the common time period at each station for the four satellite products, the assessment was focused on the common data from all the stations. The CryoSat-2 had the best match with the CAA stations data with the smallest DISO, while ICESat-2 showed the least favorable match (Table I).

Based on the comprehensive assessment with OIB Quick Look, IceBird, and the CAA stations during 2018–2022, CryoSat-2 exhibited the best overall performance, and CS2SMOS showed a similar performance (Table I). The overall performance of ICESat-2 ranked third. SMOS had
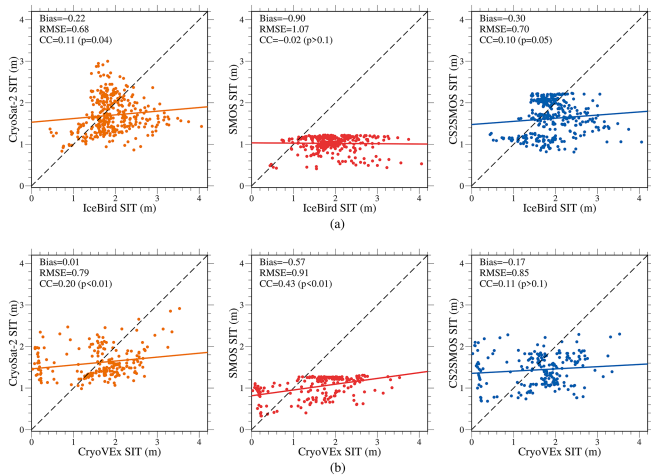
Fig. 14. Assessment of satellite SIT derived from CryoSat-2, SMOS, and CS2SMOS with (a) IceBird and (b) CroyVEx data. The dashed black line indicates the best fitting line, and the solid line indicates the scatter fitting line.

relatively large discrepancies with the airborne and in situ measurement data.

V. DISCUSSION AND CONCLUSION

The comparison and assessment results in the thinner ice region suggested that despite optimizations in the latest versions of various satellite products for SIT data, notable discrepancies persisted in the SIT retrieval. Multiple major factors contribute to the differences in SIT retrieval among various satellite products. The first major factor is the difference in measurement methods. CryoSat-2 used a radar altimeter to measure radar freeboard, primarily affected by the penetration of radar signals into the snow layer. ICESat-2 employed a laser altimeter to measure total freeboard, the combination of sea ice freeboard and snow depth, with the influence of clouds and atmospheric conditions. SMOS used a microwave radiometer to measure the brightness temperature of sea ice, which depends on the temperatures of ice, as well as its emissivity. The second major factor is the difference in the retrieval algorithm. Both CryoSat-2 and ICESat-2 derived SIT by estimating sea ice freeboard and subsequently converting it to SIT through the hydrostatic equilibrium equation. For CryoSat-2, radar freeboard can be converted to sea ice freeboard based on the correction of radar signal propagation speed in the snow layer. For ICESat-2, the total freeboard can be converted to sea ice freeboard by subtracting snow depth. While SMOS used a three layer (ocean–ice–atmosphere) dielectric slab model to derive SIT from brightness temperature. The third major factor is the difference in selected datasets and parameters. Different snow depth data were used for CryoSat-2 and ICESat-2. CryoSat-2 utilized a combination of snow depth from climatology and passive microwave remote sensing, referred to as MW99/AMSR2. ICESat-2 utilized snow depth data from the NASA Eulerian Snow On Sea Ice Model (NESOSIM). In addition, there are differences in the choice of sea ice and snow densities between CryoSat-2 and ICESat-2. For SOMS, the selections of bulk ice salinity and sea ice concentration datasets could influence the SIT retrieval.

The difference in spatial resolutions of satellite products and the selection of reference data can also affect the assessment results. Due to limited reference data, establishing an assessment that effectively evaluates monthly mean SIT products is challenging. The currently available reference data for assessment lacks the temporal extent necessary to match monthly mean satellite data. However, satellite products exhibit sparse spatial coverage over short periods, making it difficult to spatially align short-term mean satellite data with reference data. In order to ensure an adequate number of assessment points and comparability between satellite and reference data, the use of monthly mean satellite data is necessary. In addition, the measurement of these reference data can cause some uncertainties into the assessment results. The OIB L4 and OIB Quick Look datasets are radar-based, introducing significant uncertainties related to radar penetration of snow, sea ice roughness, and sidelobes. In particular, the OIB Quick Look dataset has relatively poor performance over multiyear ice and its underlying algorithm suffers from a persistent issue of misidentifying range sidelobes from the snow–ice interface as the snow–air interface. The IceBird and CryoVEx used in this study are electromagnetic datasets. The detection principle takes advantage of on the disparity in conductivity between sea ice (low conductivity) and seawater (high conductivity). However, when measuring thickness near pressure ridges, characterized by high roughness, these measurements tend to be underestimated by as much as 50%, owing to the effects of quality assurance averaging within the instrument's approximately 40-m diameter footprint.

In summary, due to the limited understanding of the performance of the latest released versions of various satellite SIT data, this study, for the first time, focused on the Arctic thinner ice region and conducted a comprehensive comparison and assessment of spatiotemporal disparities among the latest version of multisource satellite derived SIT from CryoSat-2, SMOS, CS2SMOS, and ICESat-2. The comparison and assessment of satellite data were divided into two selected periods, 2011–2022 and 2018–2022, due to the initiation of ICESat-2 data in 2018.

Over the period 2011–2022, the multiyear mean SIT of CryoSat-2, SMOS, and CS2SMOS could capture similar spatial distribution patterns in the thinner ice region. Among the three satellite products, CryoSat-2 reported the largest mean SIT, followed by CS2SMOS, and SMOS exhibited the smallest mean SIT. Notably, CS2SMOS demonstrated a closer agreement in SIT with SMOS than with CryoSat-2 in the thinner ice region. The three products reported a relatively large mean SIT in the Beaufort Sea and the East Siberian Sea and identified the Barents Sea as the subregion with the smallest mean SIT. Despite variations in certain characteristics during different seasons, the primary seasonal features generally remained consistent with those of the multiyear mean. The monthly SIT time series variations among CryoSat-2, SMOS, and CS2SMOS displayed high correlations, with all three exhibiting slight decreasing trends.

With the inclusion of ICESat-2, over the period 2018–2022, ICESat-2 recorded the largest multiyear mean SIT, followed by CryoSat-2 in the second position. CS2SMOS ranked third, and SMOS exhibited the smallest mean thickness among the four datasets. CS2SMOS maintained the closest agreement with SMOS, with the relationship between CS2SMOS and CryoSat-2
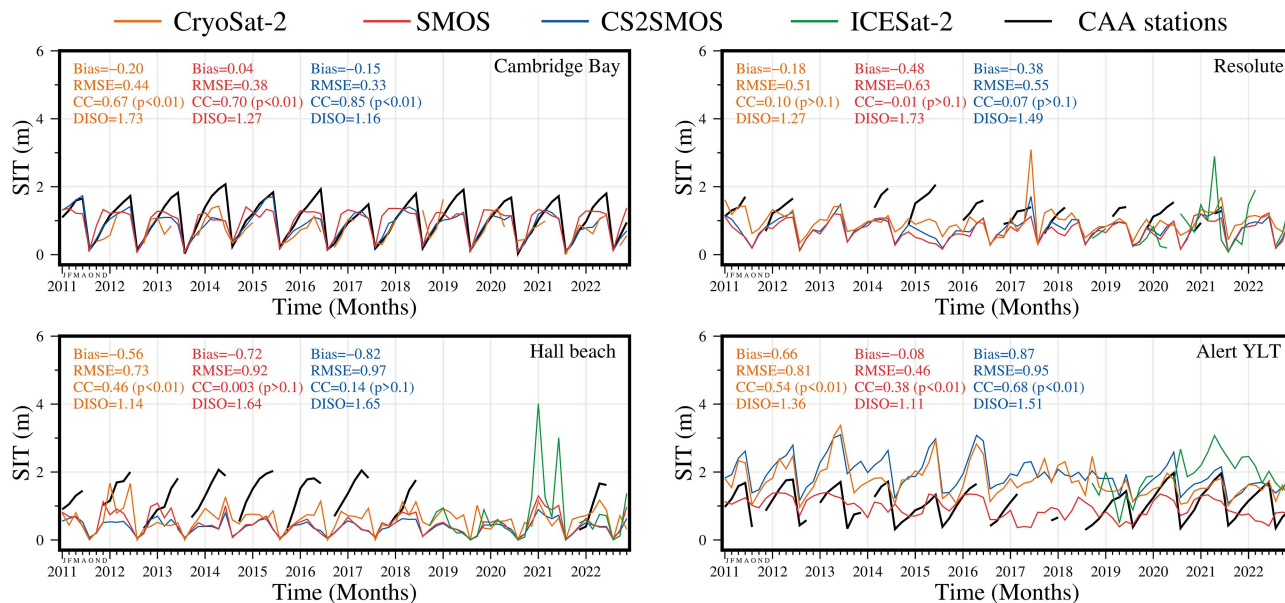
Fig. 15.   Assessment of satellite SIT derived from CryoSat-2, SMOS, CS2SMOS, and ICESat-2 with the CAA stations data.
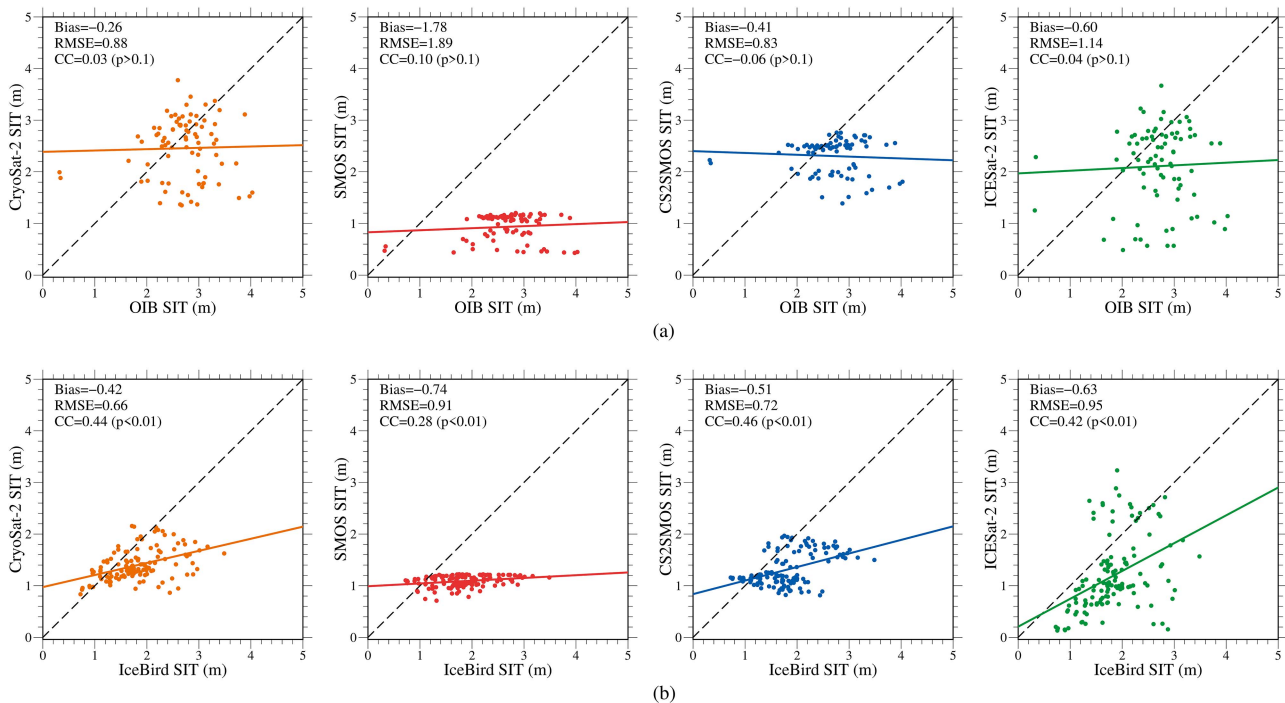

Fig. 16.   Assessment of satellite SIT derived from CryoSat-2, SMOS, CS2SMOS, and ICESat-2 with (a) OIB Quick Look and (b) IceBird data. The dashed black line indicates the best fitting line, and the solid line indicates the scatter fitting line.

being the second closest. The third closest agreement was observed between ICESat-2 and CS2SMOS. ICESat-2 exhibited similar spatiotemporal variation characteristics to the other three satellites, encompassing multiyear, seasonal, and monthly mean.

The assessment results based on various airborne and in situ measurement datasets revealed that the four satellite products generally showed some underestimations of SIT in the

thinner ice region. Over the period 2011–2022, CryoSat-2 displayed the best match of SIT with the reference datasets from OIB L4, OIB Quick Look, IceBird, CryoVEx, and the CAA stations. Therefore, a comprehensive assessment result revealed CryoSat-2 as the best overall performance product. Similarly, over the period 2018–2022, CryoSat-2 maintained the best overall performance, displaying the optimal agreement with the

datasets from OIB Quick Look, IceBird, and the CAA stations, respectively. CS2SMOS exhibited a similar performance to CryoSat-2 in the two selected periods.

In this study, the spatiotemporal comparison and assessment enhance a comprehensive understanding of the potential disparities among the latest versions of multisource satellite products, specifically focusing on the thinner ice region, contributing to a more nuanced interpretation of the observed SIT variations. These insights are crucial for the further improvement in the overall quality of satellite derived SIT data employed in climate studies and environmental monitoring. There is a note that the assessment results in the study only show the performance of satellite products within specific time periods and regions. Furthermore, inherent uncertainties are present in the reference data used. To address these limitations, future endeavors should emphasize the integration of more diverse reference data from various sources and observation methods.

REFERENCES

[1] D. K. Perovich, B. Light, H. Eicken, K. F. Jones, K. Runciman, and S. V. Nghiem, "Increasing solar heating of the arctic ocean and adjacent seas, 1979–2005: Attribution and role in the ice-albedo feedback," *Geophys. Res. Lett.*, vol. 34, no. 19, Oct. 2007, doi: 10.1029/2007GL031480.

[2] Y. Zhang et al., "Studies of the canadian arctic archipelago water transport and its relationship to basin-local forcings: Results from AO-FVCOM," *J. Geophys. Res. Oceans*, vol. 121, no. 6, pp. 4392–4415, Jun. 2016, doi: 10.1002/2016JC011634.

[3] Y. Zhang et al., "Role of sea level pressure in variations of the canadian arctic archipelago throughflow," *Adv. Climate Change Res.*, vol. 12, no. 4, pp. 539–552, Aug. 2021, doi: 10.1016/j.accre.2021.07.009.

[4] M. Sturm, D. K. Perovich, and J. Holmgren, "Thermal conductivity and heat transfer through the snow on the ice of the beaufort sea," *J. Geophys. Res. Oceans*, vol. 107, no. C10, Oct. 2002, doi: 10.1029/2000JC000409.

[5] W. N. Meier et al., "Arctic sea ice in transformation: A review of recent observed changes and impacts on biology and human activity," *Rev. Geophys.*, vol. 52, no. 3, pp. 185–217, Sep. 2014, doi: 10.1002/2013RG000431.

[6] M. G. McPhee, T. P. Stanton, J. H. Morison, and D. G. Martinson, "Freshening of the upper ocean in the arctic: Is perennial sea ice disappearing?," *Geophys. Res. Lett.*, vol. 25, no. 10, pp. 1729–1732, May 1998, doi: 10.1029/98GL00933.

[7] J. C. Stroeve et al., "Trends in Arctic sea ice extent from CMIP5, CMIP3 and observations," *Geophys. Res. Lett.*, vol. 39, no. 16, Aug. 2012, doi: 10.1029/2012GL052676.

[8] R. Kwok, "Arctic sea ice thickness, volume, and multiyear ice coverage: Losses and coupled variability (1958–2018)," *Environ. Res. Lett.*, vol. 13, no. 10, Oct. 2018, doi: 10.1088/1748-9326/aae3ec.

[9] E. Olason and D. Notz, "Drivers of variability in Arctic sea-ice drift speed," *J. Geophys. Res. Oceans*, vol. 119, no. 9, pp. 5755–5775, Sep. 2014, doi: 10.1002/2014JC009897.

[10] L. Lin, R. Lei, M. Hoppmann, D. K. Perovich, and H. He, "Changes in the annual sea ice freeze–thaw cycle in the arctic ocean from 2001 to 2018," *Cryosphere*, vol. 16, no. 12, pp. 4779–4796, Dec. 2022, doi: 10.5194/tc-16-4779-2022.

[11] Y. Zhang, X. Sun, Y. Zha, K. Wang, and C. Chen, "Changing arctic northern sea route and transpolar sea route: A prediction of route changes and navigation potential before Mid-21st century," *J. Mar. Sci. Eng.*, vol. 11, no. 12, Dec. 2023, Art. no. 2340, doi: 10.3390/jmse11122340.

[12] K. Wang, Y. Zhang, C. Chen, S. Song, and Y. Chen, "Impacts of arctic sea fog on the change of route planning and navigational efficiency in the northeast passage during the first two decades of the 21st century," *J. Mar. Sci. Eng.*, vol. 11, no. 11, Nov. 2023, Art. no. 2149, doi: 10.3390/jmse11112149.

[13] M. Johnson et al., "Evaluation of Arctic sea ice thickness simulated by arctic ocean model intercomparison project models," *J. Geophys. Res. Oceans*, vol. 117, no. C8, Aug. 2012, doi: 10.1029/2011JC007257.

[14] X. Shen et al., "Arctic sea ice variation in the northwest passage in 1979–2017 and its response to surface thermodynamics factors," *Adv. Climate Change Res.*, vol. 12, no. 4, pp. 563–580, Aug. 2021, doi: 10.1016/j.accre.2021.08.004.

[15] Y. Zhang, C. Chen, R. C. Beardsley, G. Gao, J. Qi, and H. Lin, "Seasonal and interannual variability of the Arctic sea ice: A comparison between AO-FVCOM and observations," *J. Geophys. Res. Oceans*, vol. 121, no. 11, pp. 8320–8350, Nov. 2016, doi: 10.1002/2016JC011841.

[16] I. P. Romanov, *Morphometric Characteristics of Ice and Snow in the Arctic Basin: Aircraft Landing Observations from the Former Soviet Union, 1928-1989.* vol. 1, Boulder, CO, USA: NASA National Snow and Ice Data Center Distributed Active Archive Center, 2004, doi: 10.7265/N5B8562T.

[17] D. A. Rothrock and M. Wensnahan, "The accuracy of sea ice drafts measured from U.S. navy submarines," *J. Atmospheric Ocean. Technol.*, vol. 24, no. 11, pp. 1936–1949, Nov. 2007, doi: 10.1175/JTECH2097.1.

[18] J. A. Richter-Menge, D. K. Perovich, B. C. Elder, K. Claffey, I. Rigor, and M. Ortmeyer, "Ice mass-balance buoys: A tool for measuring and attributing changes in the thickness of the arctic sea-ice cover," *Ann. Glaciol.*, vol. 44, pp. 205–210, 2006, doi: 10.3189/172756406781811727.

[19] N. Kurtz et al., "Sea ice thickness, freeboard, and snow depth products from operation icebridge airborne data," *Cryosphere*, vol. 7, no. 4, pp. 1035–1056, Jul. 2013, doi: 10.5194/tc-7-1035-2013.

[20] A. Pfaffling, C. Haas, and J. E. Reid, "Direct helicopter EM — Sea-ice thickness inversion assessed with synthetic and field data," *Geophysics*, vol. 72, no. 4, pp. F127–F137, Jul. 2007, doi: 10.1190/1.2732551.

[21] H. Lyu, W. Huang, and M. Mahdianpari, "A meta-analysis of sea ice monitoring using spaceborne polarimetric SAR: Advances in the last decade," *IEEE J. Sel. Topics Appl. Earth Observ. Remote Sens.*, vol. 15, pp. 6158–6179, 2022, doi: 10.1109/JSTARS.2022.3194324.

[22] D. Demchev, L. E. B. Eriksson, A. Hildeman, and W. Dierking, "Alignment of multifrequency sAR images acquired over sea ice using drift compensation," *IEEE J. Sel. Topics Appl. Earth Observ. Remote Sens.*, vol. 16, pp. 7393–7402, 2023, doi: 10.1109/JSTARS.2023.3302576.

[23] R. Wang, W. Zhu, X. Zhang, Y. Zhang, and J. Zhu, "Comparison of doppler-derived sea ice radial surface velocity measurement methods from sentinel-1A IW data," *IEEE J. Sel. Topics Appl. Earth Observ. Remote Sens.*, vol. 16, pp. 2178–2191, 2023, doi: 10.1109/JSTARS.2023.3241978.

[24] T. Feng, X. Liu, and R. Li, "Super-resolution-aided sea ice concentration estimation from AMSR2 images by encoder–decoder networks with atrous convolution," *IEEE J. Sel. Topics Appl. Earth Observ. Remote Sens.*, vol. 16, pp. 962–973, 2023, doi: 10.1109/JSTARS.2022.3232533.

[25] H. J. Zwally et al., "ICESat's laser measurements of polar ice, atmosphere, ocean, and land," *J. Geodynamics*, vol. 34, no. 3–4, pp. 405–445, Oct.–Nov. 2002, doi: 10.1016/S0264-3707(02)00042-X.

[26] S. W. Laxon et al., "CryoSat-2 estimates of Arctic sea ice thickness and volume," *Geophys. Res. Lett.*, vol. 40, no. 4, pp. 732–737, Feb. 2013, doi: 10.1002/grl.50193.

[27] S. Mecklenburg et al., "ESA's soil moisture and ocean salinity mission: Mission performance and operations," *IEEE Trans. Geosci. Remote Sens.*, vol. 50, no. 5, pp. 1354–1366, May 2012, doi: 10.1109/TGRS.2012.2187666.

[28] R. Ricker, S. Hendricks, L. Kaleschke, X. Tian-Kunze, J. King, and C. Haas, "A weekly Arctic sea-ice thickness data record from merged CryoSat-2 and SMOS satellite data," *Cryosphere*, vol. 11, no. 4, pp. 1607–1623, Jul. 2017, doi: 10.5194/tc-11-1607-2017.

[29] T. Markus et al., "The ice, cloud, and land elevation satellite-2 (ICESat-2): Science requirements, concept, and implementation," *Remote Sens. Environ.*, vol. 190, pp. 260–273, Mar. 2017, doi: 10.1016/j.rse.2016.12.029.

[30] G. A. Maykut, "Energy exchange over young sea ice in the central arctic," *J. Geophys. Res. Oceans*, vol. 83, no. C7, pp. 3646–3658, Jul. 1978, doi: 10.1029/JC083iC07p03646.

[31] X. Wang, J. Key, R. Kwok, and J. Zhang, "Comparison of arctic sea ice thickness from satellites, aircraft, and PIOMAS data," *Remote Sens.*, vol. 8, no. 9, Aug. 2016, Art. no. 713, doi: 10.3390/rs8090713.

[32] H. Sallila, S. L. Farrell, J. McCurry, and E. Rinne, "Assessment of contemporary satellite sea ice thickness products for Arctic sea ice," *Cryosphere*, vol. 13, no. 4, pp. 1187–1213, Apr. 2019, doi: 10.5194/tc-13-1187-2019.

[33] A. A. Petty, N. T. Kurtz, R. Kwok, T. Markus, and T. A. Neumann, "Winter arctic sea ice thickness from ICESat-2 freeboards," *J. Geophys. Res. Oceans*, vol. 125, no. 5, pp. 127–156, May 2020, doi: 10.1029/2019JC015764.

[34] M. Li, C. Ke, H. Xie, X. Miao, X. Shen, and W. Xia, "Arctic sea ice thickness retrievals from CryoSat-2: Seasonal and interannual comparisons of three different products," *Int. J. Remote Sens.*, vol. 41, no. 1, pp. 152–170, Jan. 2020, doi: 10.1080/01431161.2019.1637961.

[35] X. Shen, C. Ke, Q. Wang, J. Zhang, L. Shi, and X. Zhang, "Assessment of arctic sea ice thickness estimates from ICESat-2 using icebird airborne measurements," *IEEE Trans. Geosci. Remote Sens.*, vol. 59, no. 5, pp. 3764–3775, May 2021, doi: 10.1109/TGRS.2020.3022945.

[36] C. Soriot, C. Prigent, C. Jimenez, and F. Frappart, "Arctic sea ice thickness estimation from passive microwave satellite observations between 1.4 and 36 GHz," *Earth Space Sci.*, vol. 10, no. 2, Feb. 2023, Art. no. e2022EA002542, doi: 10.1029/2022EA002542.

[37] Y. Zhang et al., "Reconstructing long-term arctic sea ice freeboard, thickness, and volume changes from envisat, CryoSat-2, and ICESat-2," *J. Mar. Sci. Eng.*, vol. 11, no. 5, May 2023, Art. no. 979, doi: 10.3390/jmse11050979.

[38] F. Chen, D. Wang, Y. Zhang, Y. Zhou, and C. Chen, "Intercomparisons and evaluations of satellite-derived arctic sea ice thickness products," *Remote Sens.*, vol. 16, no. 3, Jan. 2024, Art. no. 508, doi: 10.3390/rs16030508.

[39] S. Hendricks and S. Paul, *Product User Guide & Algorithm Specification - AWI Cryosat-2 Sea Ice Thickness (Version 2.6)*. Genève, Switzerland: Zenodo, 2023, doi: 10.5281/zenodo.10044554.

[40] X. Tian-Kunze et al., "SMOS-derived thin sea ice thickness: Algorithm baseline, product specifications and initial verification," *Cryosphere*, vol. 8, no. 3, pp. 997–1018, May 2014, doi: 10.5194/tc-8-997-2014.

[41] A. A. Petty, N. Kurtz, R. Kwok, T. Markus, T. A. Neumann, and N. Keeney, *ICESat-2 L4 Monthly Gridded Sea Ice Thickness, Version 3*. Boulder, CO, USA: NASA National Snow and Ice Data Center Distributed Active Archive Center, 2023, doi: 10.5067/ZCSU8Y5U1BQW.

[42] N. Kurtz, M. Studinger, J. Harbeck, V. Onana, and D. Yi, *IceBridge L4 Sea Ice Freeboard, Snow Depth, and Thickness, Version 1*. Boulder, CO, USA: NASA National Snow and Ice Data Center Distributed Active Archive Center, 2015, doi: 10.5067/G519SHCKWQV6.

[43] N. Kurtz, M. Studinger, J. Harbeck, V. Onana, and D. Yi, *IceBridge Sea Ice Freeboard, Snow Depth, and Thickness Quick Look, Version 1*. Boulder, CO, USA: NASA National Snow and Ice Data Center Distributed Active Archive Center, 2016, doi: 10.5067/GRIXZ91DE0L9.

[44] A. Jutila, S. Hendricks, R. Ricker, L. von Albedyll, and C. Haas, *Airborne Sea Ice Parameters During the PAMARCMIP2017 Campaign in the Arctic Ocean, Version 1*. San Francisco, CA, USA: Pangaea, 2021, doi: 10.1594/PANGAEA.933883.

[45] A. Jutila, S. Hendricks, R. Ricker, L. von Albedyll, and C. Haas, *Airborne Sea Ice Parameters During the IceBird Winter 2019 Campaign in the Arctic Ocean, Version 1*. San Francisco, CA, USA: Pangaea, 2021, doi: 10.1594/PANGAEA.933912.

[46] S. Hendricks, R. Ricker, and A. Jutila, "ICESat-2 validation data acquisition report," AWI, Bremerhaven, Bremen, Germany, *Tech. Rep.*, Aug. 2019.

[47] C. Haas and J. Beckers, "Deliverable 6: CryoVEx 2014 final report," York Univ., Toronto, Canada, Tech. Rep. ESA 4000110552/14/MP/vb, Apr. 2015.

[48] L. Li, H. Chen, and L. Guan, "Retrieval of snow depth on arctic sea ice from the FY3B/MWRI," *Remote Sens.*, vol. 13, no. 8, Apr. 2021, Art. no. 1457, doi: 10.3390/rs13081457.

[49] R. Kwok and G. F. Cunningham, "Variability of arctic sea ice thickness and volume from CryoSat-2," *Philos. Trans. Roy. Soc. A: Math., Phys. Eng. Sci.*, vol. 373, no. 2045, Jul. 2015, doi: 10.1098/rsta.2014.0157.

[50] R. Kwok, S. Kacimi, M. A. Webster, N. T. Kurtz, and A. A. Petty, "Arctic snow depth and sea ice thickness from ICESat-2 and CryoSat-2 freeboards: A first examination," *J. Geophys. Res. Oceans*, vol. 125, no. 3, Mar. 2020, doi: 10.1029/2019JC016008.

[51] Z. Hu et al., "CCHZ-DISO: A timely new assessment system for data quality or model performance from da dao zhi jian," *Geophys. Res. Lett.*, vol. 49, no. 23, Dec. 2022, doi: 10.1029/2022GL100681.

Guohao Li received the B.E. degree in marine resource development technology from Lingnan Normal University, Zhanjiang, China, in 2022. He is currently working toward the M.S. degree in marine science with the College of Oceanography and Ecological Science, Shanghai Ocean University, Shanghai, China.

His research interests include remote sensing, numerical models, sea ice variation, and polar oceanography.

Huan Li received the B.S. degree in geographic information science from the Suzhou University of Science and Technology, Suzhou, China, in 2023. She is currently working toward the M.S. degree in marine science with the College of Oceanography and Ecological Science, Shanghai Ocean University, Shanghai, China.

Her research interests include remote sensing, machine learning, numerical models, polar oceanography, and climate change.

Changsheng Chen received the M.S. degree in marine meteorology from the Ocean University of China, Qingdao, China, in 1983, and the M.S. and Ph.D. degrees in physical oceanography from the Massachusetts Institute of Technology, Cambridge, MA, USA, in 1989 and 1992, respectively.

In 1992, he was a Postdoctoral Researcher with Woods Hole Oceanographic Institution, Falmouth, MA, USA. From 1992 to 1994, he was a Research Scientist with Texas A&M University, College Station, TX, USA. From 1994 to 2001, he was an Assistant Professor and Associate Professor with the University of Georgia, Athens, GA, USA. In 2001, he joined the School for Marine Science and Technology, University of Massachusetts-Dartmouth, North Dartmouth, MA, USA, as a Full Professor. He is currently the Montgomery Charter Chair Professor and Commonwealth Professor with the University of Massachusetts-Dartmouth. His research interests include polar oceanography, multiscaling ocean model developments, climate change, modeling and observational exploration of coastal ocean circulation, oceanic frontal processes, and biological and physical interactions.

Yu Zhang (Member, IEEE) received the B.S. degree in physics from East China Normal University, Shanghai, China, in 2009, and the Ph.D. degree in marine science and technology from the University of Massachusetts-Dartmouth, North Dartmouth, MA, USA, in 2016.

From 2016 to 2019, he was an Assistant Professor with the College of Oceanography and Ecological Science, Shanghai Ocean University, Shanghai, China, where he has been an Associate Professor with the College of Marine Sciences. His research interests include physical oceanography, air–sea–ice interactions, climate change, remote sensing, and numerical models.

Weizeng Shao (Member, IEEE) received the B.S. degree in engineering from the JiangSu University of Science and Technology, Zhenjiang, China, in 2007, and the Ph.D. degree in physical oceanography from the Ocean University of China, Qingdao, China, in 2013.

During his Ph.D. program from 2010 to 2012, he was a Visiting Research Scientist with the SAR oceanography group, German Aerospace Center, Munich, Germany. During 2015−2020, he was an Associate Professor with Zhejiang Ocean University, Zhoushan, China. Since 2019, he has been an Assistant Researcher with the National Satellite Ocean Application Service, Beijing, China. Since 2021, he has been a Full Professor with Shanghai Ocean University, Shanghai, China. His research interests include marine applications of synthetic aperture radar, especially from Chinese Gaofen-3, HY-2, and CFOSAT, and ocean modeling of typhoons and hurricanes.

Yi Zhou received the B.S. degree in marine science from Shanghai Ocean University, Shanghai, China, in 2023. He is currently working toward the Ph.D. degree in physical oceanography with the School of Oceanography, Shanghai Jiao Tong University, Shanghai.

His research interests include polar remote sensing, Arctic sea ice, snow depth, and physical process of sea ice.

Deshuai Wang received the B.S. degree in marine science from Ocean University of China, Qingdao, China, in 2011, the M.S. degree in marine science from the National Marine Environmental Forecasting Center, Beijing, China, in 2014, and the Ph.D. degree in marine science and technology from the University of Massachusetts-Dartmouth, North Dartmouth, MA, USA, in 2022.

Since 2022, he has been a Research Scientist with the University of Maryland Center for Environmental Science, Cambridge, MD, USA. His research interests include numerical models, remote sensing, polar oceanography, sea ice, and climate change.